2D Materials

LETTER • OPEN ACCESS

Comeback of epitaxial graphene for electronics: large-area growth of bilayer-free graphene on SiC

To cite this article: Mattias Kruskopf *et al* 2016 *2D Mater.* **3** 041002

View the article online for updates and enhancements.

Related content

- Epitaxial graphene on SiC: modification of structural and electron transport properties by substrate pretreatment
Mattias Kruskopf, Klaus Pierz, Stefan Wundrack et al.

- Combining graphene with silicon carbide: synthesis and properties – a review
Ivan Shtepliuk, Volodymyr Khranovskyy and Rositsa Yakimova

- Charged nano-domes and bubbles in epitaxial graphene
A Ben Gouider Trabelsi, F V Kusmartsev, B J Robinson et al.

Recent citations

- Transport properties of graphene films grown by thermodestruction of SiC (0001) surface in argon medium
S. P. Lebedev *et al*

- Graphene, microscale metallic mesh, and transparent dielectric hybrid structure for excellent transparent electromagnetic interference shielding and absorbing
Zhengang Lu *et al*

This content was downloaded from IP address 194.95.157.206 on 15/01/2018 at 14:04

2D Materials

OPEN ACCESS

RECEIVED
28 June 2016

REVISED
25 August 2016

ACCEPTED FOR PUBLICATION
13 September 2016

PUBLISHED
27 September 2016

Original content from this work may be used under the terms of the Creative Commons Attribution 3.0 licence.

Any further distribution of this work must maintain attribution to the author(s) and the title of the work, journal citation and DOI.

LETTER

Comeback of epitaxial graphene for electronics: large-area growth of bilayer-free graphene on SiC

Mattias Kruskopf[1], Davood Momeni Pakdehi[1], Klaus Pierz[1], Stefan Wundrack[1], Rainer Stosch[1], Thorsten Dziomba[1], Martin Götz[1], Jens Baringhaus[2], Johannes Aprojanz[2], Christoph Tegenkamp[2], Jakob Lidzba[3], Thomas Seyller[3], Frank Hohls[1], Franz J Ahlers[1] and Hans W Schumacher[1]

[1] Physikalisch-Technische Bundesanstalt, Bundesallee 100, D-38116 Braunschweig, Germany
[2] Institute of Solid State Physics of Leibniz Universität Hannover, Appelstraße 2, D-30167 Hannover, Germany
[3] Institute of Physics of Technische Universität Chemnitz, Reichenhainer Straße 70, D-09126 Chemnitz, Germany

E-mail: Mattias.Kruskopf@ptb.de and Klaus.Pierz@ptb.de

Keywords: epitaxial graphene on SiC, quantum Hall effect, buffer layer, bilayer free, large scale, suppression of step bunching, carbon deposition

Supplementary material for this article is available online

Abstract

We present a new fabrication method for epitaxial graphene on SiC which enables the growth of ultra-smooth defect- and bilayer-free graphene sheets with an unprecedented reproducibility, a necessary prerequisite for wafer-scale fabrication of high quality graphene-based electronic devices. The inherent but unfavorable formation of high SiC surface terrace steps during high temperature sublimation growth is suppressed by rapid formation of the graphene buffer layer which stabilizes the SiC surface. The enhanced nucleation is enforced by decomposition of deposited polymer adsorbate which acts as a carbon source. Unique to this method are the conservation of mainly 0.25 and 0.5 nm high surface steps and the formation of bilayer-free graphene on an area only limited by the size of the sample. This makes the polymer-assisted sublimation growth technique a promising method for commercial wafer scale epitaxial graphene fabrication. The extraordinary electronic quality is evidenced by quantum resistance metrology at 4.2 K showing ultra-high precision and high electron mobility on mm scale devices comparable to state-of-the-art graphene.

Introduction

The success of graphene as a basis for new applications crucially depends on the reliability of the available technologies to fabricate large areas of homogenous high quality graphene layers. Epitaxial growth on metals as well as on SiC substrates is employed with specific benefits and drawbacks. Single graphene layers epitaxially grown on SiC offer a high potential for electronic device applications [1]. They combine excellent properties, e.g. high electron mobilities, with the opportunity for wafer-scale fabrication and direct processing on semi-insulating substrates without the need to transfer the graphene to a suitable substrate [2]. Some progress has been achieved during the recent years. In particular, high temperature sublimation growth under Ar atmosphere [3, 4] or by confinement control [5, 6] significantly improved the uniformity of of the graphene domains on SiC substrates. The coverage of graphene bilayers could be reduced from wide stripes formed along the terraces to micrometer-sized bilayer patches [7]. Furthermore, it was found that beyond pure sublimation growth from SiC, graphene formation can be assisted by additional carbon supply from external sources [8, 9]. In particular, by using propane in a chemical vapor deposition process the versatility of the graphene growth is improved [10, 11].

However, in spite of the progress achieved so far, the growth of high quality graphene in a reproducible manner remains challenging [12]. The problem of the inherent high step edge formation caused by step bunching of the SiC substrate is not solved, leading to an increased electrical resistance [13, 14] and anisotropic electronic properties [15, 16]. Irregular step heights are usually connected to graphene bilayer

© 2016 IOP Publishing Ltd

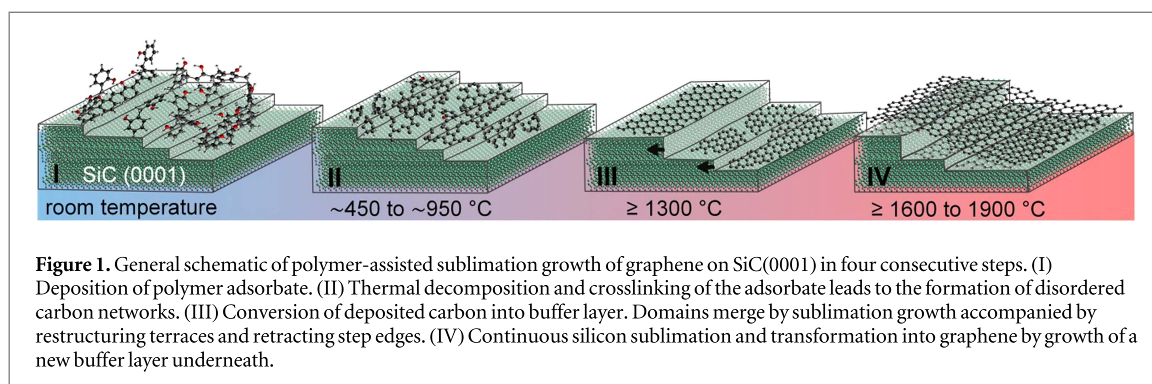

Figure 1. General schematic of polymer-assisted sublimation growth of graphene on SiC(0001) in four consecutive steps. (I) Deposition of polymer adsorbate. (II) Thermal decomposition and crosslinking of the adsorbate leads to the formation of disordered carbon networks. (III) Conversion of deposited carbon into buffer layer. Domains merge by sublimation growth accompanied by restructuring terraces and retracting step edges. (IV) Continuous silicon sublimation and transformation into graphene by growth of a new buffer layer underneath.

formation with a surface coverage of a few percent. Those metallic bilayer patches can short-circuit closely spaced contacts and can severely deteriorate the electronic properties [17–19]. These drawbacks so far have delayed the implementation of SiC sublimation growth for wafer-scale device fabrication.

Here we describe a new sublimation growth method that leads to the formation of bilayer-free graphene on SiC with exceptionally shallow step heights and a layer size which is only limited by the dimensions of the sample. The core of this method is to seed the growth of the surface stabilizing buffer layer by an external carbon source before the smooth surface morphology is destroyed by step bunching occurring at high temperature annealing. A simple and effective implementation of this idea is the deposition of a polymer on the SiC substrate which then assists the formation of the buffer layer. The process of what we call polymer-assisted sublimation growth (PASG) of graphene on SiC is schematically depicted in figure 1 and comprises four steps: (I) deposition of the polymer adsorbate, (II) decomposition into amorphous carbon and nanocrystalline graphite, (III) conversion into buffer layer domains and (IV) closing of the buffer layer and graphene growth by high temperature sublimation growth.

Enhanced buffer layer nucleation from graphite nanocrystals

For PASG a phenolic resin was deposited onto the sample surface by dipping and rinsing (see methods) which results in a homogenous distribution of a droplet-like adsorbate with structure heights of usually up to 20 nm depending on the preparation conditions. Figure 2(a) shows a typical topography after polymer deposition. No structural changes could be identified in the Raman spectrum of the adsorbate (figure 2(k)) upon vacuum annealing up to about 300 °C. This indicates a high thermal stability of the resin as it was described by Ko *et al* [21]. When the annealing temperature exceeds $T_a = 450$ °C, a disordered carbon network including sp^2-hybridized hexagonal carbon rings appears due to crosslinking of the phenolic resin. This is indicated by the two broad Raman bands known as the *D*- and *G*- peaks, emerging at around 1360 and 1590 cm^{-1}, respectively (figure 2(k)) [20, 21]. In addition, the x-ray photoemission spectrum (XPS) (figure 2(l) bottom) shows an emerging band upon annealing at 450 °C which can be fitted by two Gaussian curves indicating the presence of two components (*A*1 and *A*2). The peak positions occur at higher binding energies $\Delta E_{A1} = 1.80$ eV and $\Delta E_{A2} = 2.70$ eV with respect the SiC bulk component. The peak positions of the SiC bulk components of the spectra in figure 2(l) are aligned to the literature value of 283.7 eV [22]. The separation of (0.9 ± 0.1) eV between A_1 and A_2 is in good agreement with that of the sp^2 and sp^3 hybridized forms of carbon [23]. The appearance of both bonding types indicates the amorphous nature of the carbon network. The relative portion of sp^3 bonds was estimated to be ~17% from the intensity ratio of the two XPS-components regarding the measurement procedure explained by Díaz *et al* [23]. This is comparable with ~10% determined from the Raman spectrum, see supplementary information [20].

The AFM image in figure 2(b) shows that after annealing at $T_a = 950$ °C the structure heights observed in figure 2(a) are significantly reduced to ⩽0.75 nm and parallel terraces with a height of 0.25 nm are revealed. This step and terrace structure is already known from the clean CMP wafer surface before processing. However, AFM measurements indicate an increase in the roughness compared to clean substrates which is assigned to carbon networks from the decomposed polymer. The (1 × 1) low energy electron diffraction (LEED) pattern of the sample proves that up to this point the carbon is not converted into buffer layer (figure 2(i)). By following the interpretation of Raman spectra of disordered carbon of Ferrari and Robertson [20] the carbon network is best described by nanocrystalline graphite clusters when reaching 950 °C (figure 2(k)). An assignment of the clusters to glassy carbon is ruled out by the existence of sp^3 carbon bonds [24, 25] as well as the missing 2*D* peak in the Raman spectra [26, 27].

The conversion of the carbon clusters into the buffer layer starts at $T_a \approx 1300$ °C which is about 100 K lower compared to the buffer layer growth on clean

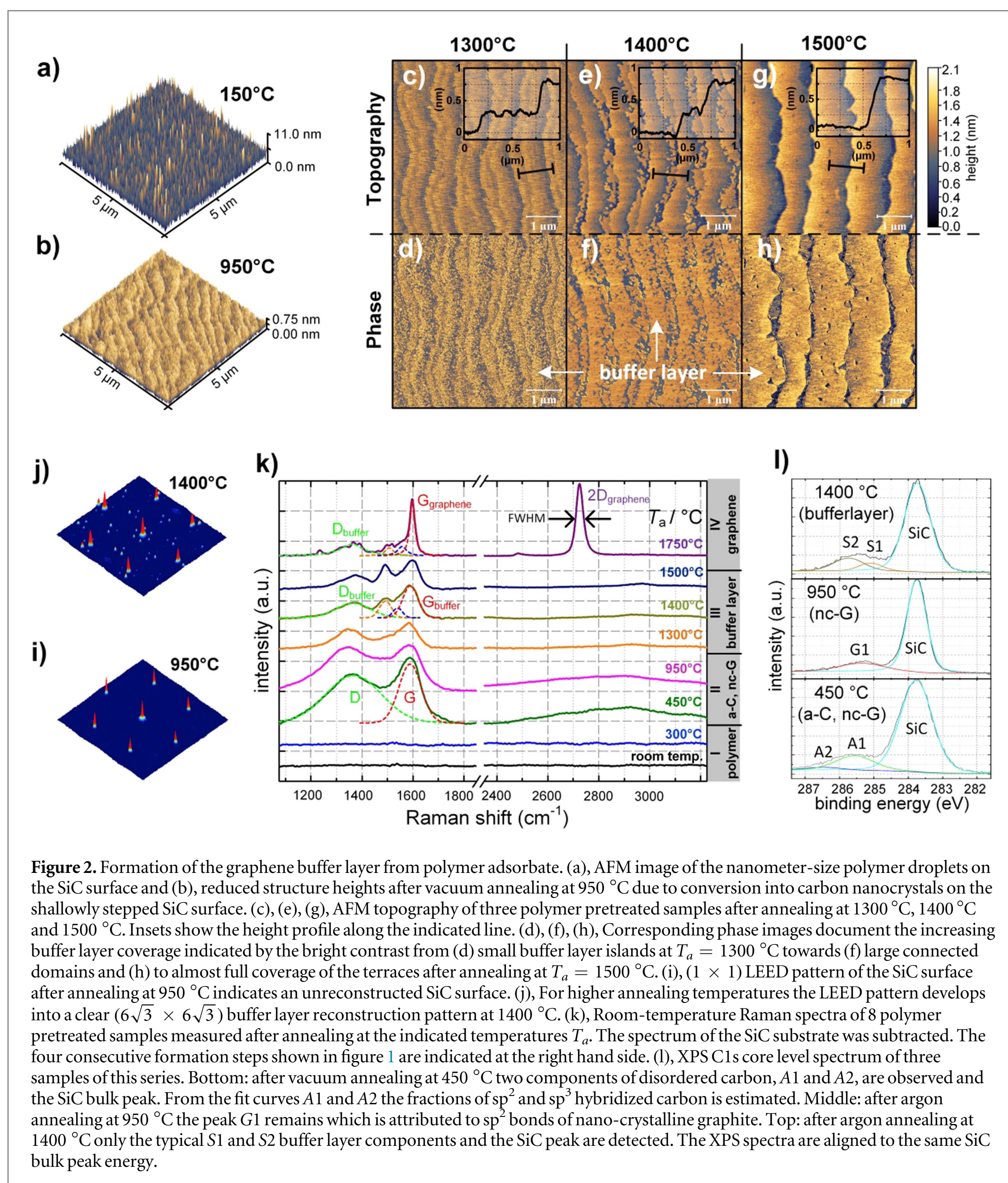

Figure 2. Formation of the graphene buffer layer from polymer adsorbate. (a), AFM image of the nanometer-size polymer droplets on the SiC surface and (b), reduced structure heights after vacuum annealing at 950 °C due to conversion into carbon nanocrystals on the shallowly stepped SiC surface. (c), (e), (g), AFM topography of three polymer pretreated samples after annealing at 1300 °C, 1400 °C and 1500 °C. Insets show the height profile along the indicated line. (d), (f), (h), Corresponding phase images document the increasing buffer layer coverage indicated by the bright contrast from (d) small buffer layer islands at T_a = 1300 °C towards (f) large connected domains and (h) to almost full coverage of the terraces after annealing at T_a = 1500 °C. (i), (1×1) LEED pattern of the SiC surface after annealing at 950 °C indicates an unreconstructed SiC surface. (j), For higher annealing temperatures the LEED pattern develops into a clear $(6\sqrt{3} \times 6\sqrt{3})$ buffer layer reconstruction pattern at 1400 °C. (k), Room-temperature Raman spectra of 8 polymer pretreated samples measured after annealing at the indicated temperatures T_a. The spectrum of the SiC substrate was subtracted. The four consecutive formation steps shown in figure 1 are indicated at the right hand side. (l), XPS C1s core level spectrum of three samples of this series. Bottom: after vacuum annealing at 450 °C two components of disordered carbon, $A1$ and $A2$, are observed and the SiC bulk peak. From the fit curves $A1$ and $A2$ the fractions of sp^2 and sp^3 hybridized carbon is estimated. Middle: after argon annealing at 950 °C the peak $G1$ remains which is attributed to sp^2 bonds of nano-crystalline graphite. Top: after argon annealing at 1400 °C only the typical $S1$ and $S2$ buffer layer components and the SiC peak are detected. The XPS spectra are aligned to the same SiC bulk peak energy.

SiC surfaces without polymer assistance [4, 28]. At this temperature a weak LEED pattern of a $(6\sqrt{3} \times 6\sqrt{3})$ surface reconstruction is observed which at 1400 °C turns into a clear pattern shown in figure 2(j). This indicates a trend towards the formation of connected buffer layer domains, also documented by the change of the vibrational modes in the Raman spectra starting around 1300 °C (figure 2(k)). Most of the hydrogen and oxygen atoms from the deposited polymer are expected to be desorbed at this stage, see supplementary information. In the temperature range 1400 °C–1500 °C an additional set of Raman bands (around 1370, 1492, 1543 and 1595 cm^{-1}) becomes clearly visible which can be assigned to the vibrational density of states of the $(6\sqrt{3} \times 6\sqrt{3})$ surface reconstruction [28]. This is also confirmed by the corresponding XPS spectrum (figure 2(l) top) showing the typical $S1$ and $S2$ components of the buffer layer at (1.36 ± 0.15) eV and (2.00 ± 0.19) eV with respect to the SiC-bulk peak position [22]. Both components are attributed to the sp^2-bonded C atoms of the buffer layer ($S2$) and those which are bonded to a Si atom ($S1$) of the underlying SiC layer [22]. The excellent fit of the XPS spectrum by the $S1$ and $S2$ peaks gives no indication of another peak, e.g. a residual $G1$ component which has been observed at lower temperatures and has been attributed to nanocrystalline graphite clusters. It is therefore expected that the graphite clusters resolved into carbon which is incorporated into the buffer layer.

The evolution of the buffer layer and the terrace structure is visualized by AFM measurements taken

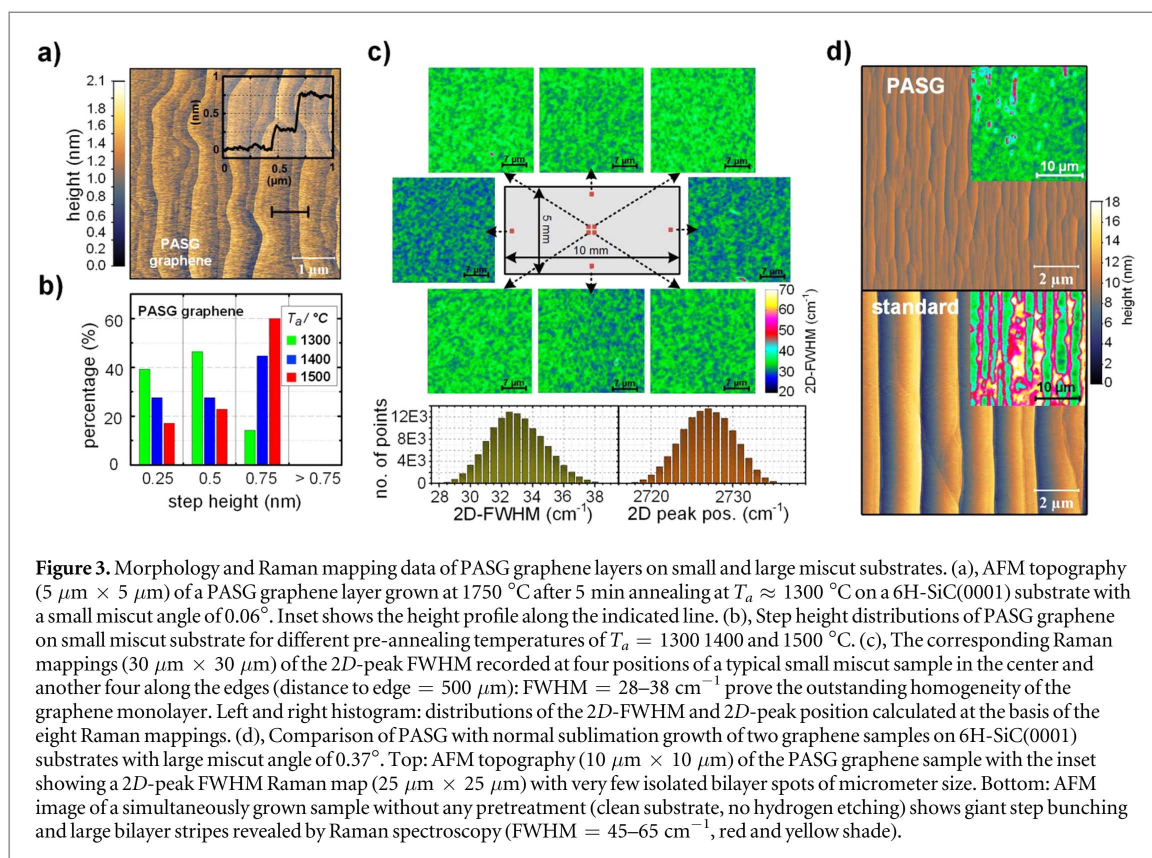

Figure 3. Morphology and Raman mapping data of PASG graphene layers on small and large miscut substrates. (a), AFM topography (5 μm × 5 μm) of a PASG graphene layer grown at 1750 °C after 5 min annealing at $T_a \approx$ 1300 °C on a 6H-SiC(0001) substrate with a small miscut angle of 0.06°. Inset shows the height profile along the indicated line. (b), Step height distributions of PASG graphene on small miscut substrate for different pre-annealing temperatures of T_a = 1300 1400 and 1500 °C. (c), The corresponding Raman mappings (30 μm × 30 μm) of the 2D-peak FWHM recorded at four positions of a typical small miscut sample in the center and another four along the edges (distance to edge = 500 μm): FWHM = 28–38 cm^{-1} prove the outstanding homogeneity of the graphene monolayer. Left and right histogram: distributions of the 2D-FWHM and 2D-peak position calculated at the basis of the eight Raman mappings. (d), Comparison of PASG with normal sublimation growth of two graphene samples on 6H-SiC(0001) substrates with large miscut angle of 0.37°. Top: AFM topography (10 μm × 10 μm) of the PASG graphene sample with the inset showing a 2D-peak FWHM Raman map (25 μm × 25 μm) with very few isolated bilayer spots of micrometer size. Bottom: AFM image of a simultaneously grown sample without any pretreatment (clean substrate, no hydrogen etching) shows giant step bunching and large bilayer stripes revealed by Raman spectroscopy (FWHM = 45–65 cm^{-1}, red and yellow shade).

from a series of three samples that were annealed for 5 min at T_a = 1300, 1400 or 1500 °C in Ar atmosphere, respectively (figures 2(c)–(h)). The topographic AFM image (figure 2(c)) shows that at 1300 °C regular facets with step heights of 0.25 nm and 0.5 nm evolve. The dense layer of nanometer size bright spots observed in the AFM phase contrast image (figure 2(d)) is attributed to the first buffer layer domains detected by LEED. The high density of graphite nanocrystals is crucial to the rapid formation of these small domains at 1300 °C since they provide carbon and act as preferred nuclei for diffusing carbon atoms released by the restructuring terraces. This enhanced buffer layer nucleation reduces the diffusion length of the released carbon atoms and makes an unhindered mass transport between the terrace edges more difficult or nearly impossible. In the kinetic approach of the giant step bunching mechanism, however, an interaction between terrace edges is necessary to mediate the rebuilding of the terrace structure and the bunching of the steps [29] as it is the case for clean SiC surfaces. Thus, the main reasons for the success of PASG are the uniform nucleation of homogenously distributed buffer layer domains and the suppression of mass transport mechanisms on the surface that are critical during giant step formation.

A significantly higher annealing temperature of about 1400 °C is needed to initiate decomposition of the shallow 0.25 nm terraces (figure 2(e)) and 1500 °C to reach the next stable step configuration with heights of 0.75 nm (figure 2(g)). The reason for the relatively slow step velocity of the retracting crystal planes is the rapidly formed buffer layer which stabilizes the surface by surface free energy minimization due to the formation of covalent bonds to the substrate [30]. These bonds on the SiC (0001) plane also ensure that there is only one rotational orientation of the buffer layer lattice with respect to the lattice of the substrate [4] as indicated by the spotty LEED pattern of the buffer layer after annealing at 1400 °C in figure 2(j). As a result separated buffer layer domains merge without forming grain boundaries. The released carbon from the decomposition of the SiC step edges at higher temperatures of 1400 °C and 1500 °C supports buffer layer growth and helps to close the gaps as indicated by the corresponding AFM images in figure 2(c)–(h). The AFM images show also that with increasing temperature the rough edges of the decomposing SiC terraces become smooth which is supposed to be an excellent template for graphene growth.

Bilayer-free graphene growth on ultra-shallow terraces

Monolayer graphene growth was performed on substrates with a small miscut angle (~0.05°) by pre-annealing at T_a = 1300 °C followed by heating (~400 K min^{-1}) the sample to 1750 °C. This fast heating rate ensures that the critical temperature window between ~1300 °C and ~1500 °C is passed rapidly (in about 30 s) before step bunching can lead to

the formation of 0.75 nm high step edges which needs about 5 min at 1500 °C as shown in figure 2(g).

Indeed, the AFM topography (figure 3(a)) shows a very regular surface morphology without gaps in the resulting graphene layer. Smooth terrace edges are observed where about 85% of the step heights correspond to a sequence of 0.25 or 0.5 nm. These heights correspond to one or two SiC bilayers, respectively. The absence of heights larger than 0.75 nm is unique to this method. The step height histogram (figure 3(b)) reveals that for buffer layer formation at higher annealing temperatures of 1400 °C (blue) or 1500 °C (red) the fraction of steps with heights <0.75 nm decreases to 54% and 40%, respectively. This correlation indicates that the final step height found after graphene formation can be traced back to the one which was predefined during the annealing step. The rapidly preformed buffer layer achieved by PASG is the reason for the surface stabilization which is known to reduce step velocities and conserve step heights [19, 31]. This prevents restructuring of the SiC surface and a large number of the preformed shallow single and double SiC bilayer steps remain during the high temperature graphitization at 1750 °C

The Raman spectrum after graphene formation (figure 2(k)) contains the typical Lorentzian-shaped G-peak at 1598 cm^{-1} and a 2D-peak at 2724 cm^{-1} with a narrow full-width at half-maximum (FWHM) of 33 cm^{-1} proving the presence of a monolayer [32]. The broad D-peak labeled as D_{buffer} around 1350 cm^{-1}, is attributed to the buffer layer below the graphene [28]. This is the signal of the new buffer layer which converts the formerly PASG buffer layer into the graphene layer by separating it from the bonds of the SiC substrate [22, 33]. In the range between 1200 and 1400 cm^{-1} several additional very small peaks superimpose the broad D_{buffer} peak. A very similar Raman difference spectrum was also found for step flow grown mono-layer graphene on SiC [34]. It was proposed that the peak at about 1230 cm^{-1} could be due to the vibrational density of states of the buffer layer while the weak but noticeable narrow signals near 1350 cm^{-1} are expected to be related to a graphene D-peak [34]. The very small intensity indicates a very low defect density in the hexagonal 2D graphene lattice which is comparable to step-flow grown graphene layers [34, 35].

The outstanding homogeneity of the PASG graphene is demonstrated by micro-Raman area mappings (each 30 μm × 30 μm) recorded in the center and 500 μm away from the edges of the 5 mm × 10 mm sample. The mappings of the 2D-band FWHM values (figure 3(c)) scatter over a narrow range (blue/green color) between 28 and 38 cm^{-1} around a mean value of 33 cm^{-1}. The micro-Raman mappings support the AFM measurements since both methods show that a continuous graphene layer has formed without gaps. The histogram of the FWHM values in figure 3(c), (left histogram) shows a Gaussian-like distribution with a central FWHM value at 32.9 cm^{-1} and a standard deviation of 1.8 cm^{-1}. The measured FWHM values prove that exclusively monolayer graphene was formed [32]. This was confirmed by large scale optical microscopy inspections (see methods). Thus the sample can be considered as bilayer-free. This is a result of the uniform graphene formation by the PASG and the conservation of low step heights since high step edges are known to favor bilayer formation [4, 12, 19]. Only at substrate defects such as micropipes and in some cases very close to the sample edge bilayer patches were observed (figure S1(b), supplementary information). Furthermore, the 2D peak positions estimated from the 8 Raman mappings show a very narrow Gaussian-like distribution around 2727 cm^{-1} (standard deviation of 3.4 cm^{-1}) (figure 3(c), right histogram) compared to ~2680 cm^{-1} for exfoliated graphene. This indicates a moderate and homogenous compressive strain across the graphene layer, which is a characteristic feature for epitaxial graphene [36].

The stabilization of the steps of the SiC surface by PASG is demonstrated by using a substrate with a deliberately larger miscut angle (~0.37°) which usually shows a strong tendency towards giant step bunching at high temperatures [7]. This becomes obvious from the AFM image in figure 3(d) (bottom). After standard graphene formation without PASG a completely giant-stepped surface is formed with 1.5–2 μm wide terraces and 10–15 nm high steps over the entire surface. The corresponding Raman 2D-FWHM mapping (see inset) clearly reveals that monolayer graphene exists on the terraces while along the high terrace edges long stripes of bilayer graphene (FWHM values of 45–65 cm^{-1}) are present which is typical for graphene step flow growth [4, 37]. In contrast, an entirely different and shallow surface structure (figure 3(d), top) is obtained for a simultaneously processed graphene sample with the predefined buffer layer formed by PASG at 1400 °C. Both, the values of the terrace width (approximately ~250 nm) and the heights between 0.5 and 2.5 nm are about 10 times smaller compared to the sample without PASG treatment. Obviously, also in the case of larger miscut angles the increased surface stability achieved by the pre-formed buffer layer successfully suppresses giant step bunching and graphene step flow growth such that a homogenous coverage of monolayer graphene without bilayer stripes is obtained. On such substrates just a few isolated graphene bilayer domains are observed which can be assigned to local step height variations. This experiment demonstrates the high potential of the PASG technique for full-size SiC wafers which usually exhibit fluctuations in their miscut components.

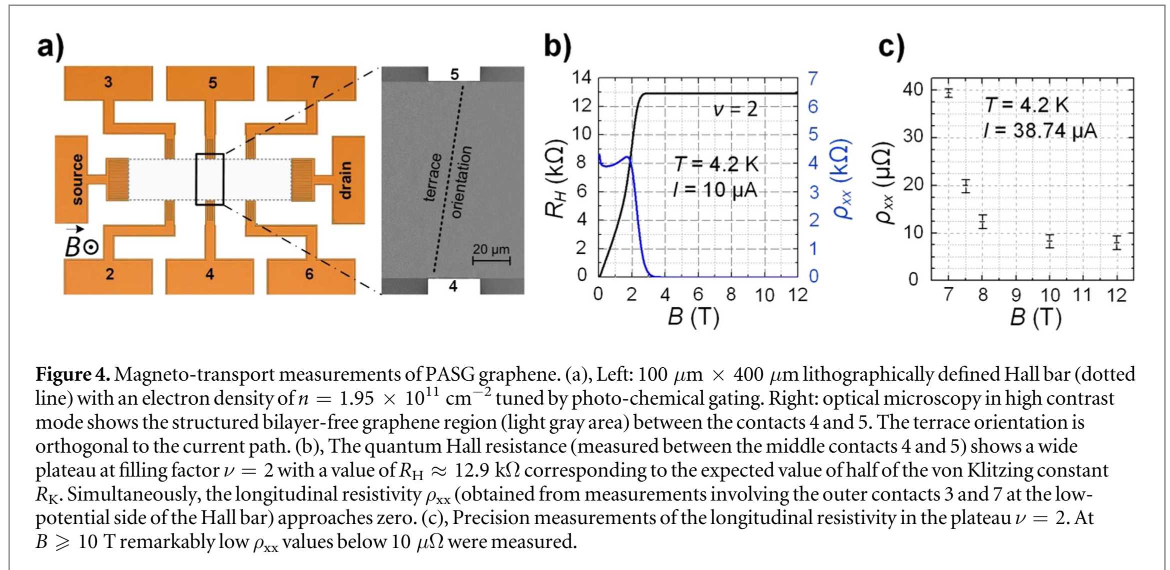

Figure 4. Magneto-transport measurements of PASG graphene. (a), Left: 100 μm $\times$ 400 μm lithographically defined Hall bar (dotted line) with an electron density of $n = 1.95 \times 10^{11}$ cm^{-2} tuned by photo-chemical gating. Right: optical microscopy in high contrast mode shows the structured bilayer-free graphene region (light gray area) between the contacts 4 and 5. The terrace orientation is orthogonal to the current path. (b), The quantum Hall resistance (measured between the middle contacts 4 and 5) shows a wide plateau at filling factor $\nu = 2$ with a value of $R_H \approx 12.9$ kΩ corresponding to the expected value of half of the von Klitzing constant R_K. Simultaneously, the longitudinal resistivity ρ_{xx} (obtained from measurements involving the outer contacts 3 and 7 at the low-potential side of the Hall bar) approaches zero. (c), Precision measurements of the longitudinal resistivity in the plateau $\nu = 2$. At $B \geqslant 10$ T remarkably low ρ_{xx} values below 10 $\mu\Omega$ were measured.

High-mobility electronic transport properties and quantum metrological device application

Finally, the electronic properties of the PASG graphene samples (on SiC substrates with small miscut angle) were examined by various transport experiments. Four-probe van der Pauw and Hall measurements were performed on squares of 4.5 mm $\times$ 4.5 mm between 2.2 K and 295 K. Measurements performed immediately after finishing graphene growth exhibit an electron mobility of $\mu = 2800$ cm^2 V^{-1} s^{-1} at room temperature and 9500 cm^2 V^{-1} s^{-1} at 2.2 K with an electron density of $n = 8.1 \times 10^{11}$ cm^{-2} and 7.5×10^{11} cm^{-2}, respectively. These results demonstrate that high mobility values can be obtained with PASG graphene even for very large devices on millimeter scale which indicates an excellent homogeneity of the samples and a very low defect density which is in good agreement with the obtained Raman measurements. Since it is known that the electronic properties of graphene can vary with the change of ambient conditions or by lithographical processing a comparison to literature values can be just a rough estimate. Similar electron mobility values were measured at millimeter-sized samples from state-of-the-art graphene grown by thermal sublimation [38, 39] and CVD [40].

The measured intrinsic electron densities below 10^{12} cm^{-2} are lower than values usually reported in the literature and close to what is desired for realizing graphene-based resistance standards. In quantum metrology the unit ohm is traced back to the fundamental constants h and e via the von Klitzing constant $R_K \equiv h/e^2$. The main advantage of graphene over a conventional GaAs/GaAlAs based two-dimensional electron system is the larger Landau-level splitting and the absence of a 2nd sub band which makes the quantum Hall effect (QHE) accessible at higher temperatures. A Hall bar was lithographically processed and aligned nearly perpendicular with respect to the terrace orientation, figure 4(a). In order to examine the quantum Hall resistance plateau at filling factor $\nu = 2$ at reasonable magnetic fields $B \leqslant 12$ T the carrier density was tuned to $n = 1.95 \times 10^{11}$ cm^{-2} by photo-chemical-gating [41]. The Hall resistance R_H and the longitudinal resistivity ρ_{xx} as functions of the magnetic flux density B were measured at 4.2 K, figure 4(b). The high quality of the graphene can be verified by precision measurements of ρ_{xx} in the plateau region since the remaining resistivity in this temperature regime is related to scattering induced by density inhomogeneities [42]. For $B > 3$ T a wide resistance plateau of 12.9 k$\Omega \approx R_K/2$ is observed and ρ_{xx} drops below 10 $\mu\Omega$ for $B \geqslant 10$ T, figure 4(c). ρ_{xx} is thus lower than any published value obtained at 4.2 K [42, 43]. This describes extremely low defect scattering and material inhomogeneities despite the perpendicularly orientated terraces with respect to the current direction. Since the 800 step edges along the Hall bar seem to have little effect, isotropic electronic properties due to the ultra-shallow step heights are expected. This confirms that the ultra-low step heights are beneficial for electronic transport [16, 17] and ideal to electronic device applications. Taking into account that the Hall voltage drop occurs between the diagonally opposing corners of a Hall contact pair [44] one can calculate from the ρ_{xx} values and the geometry of the contacts an upper limit [45] for the deviation from $R_K/2$ of the Hall resistance (see methods). The upper limit was determined for each of the three pairs of directly opposing potential contacts (figure 4(a)). At $B = 7$ T one finds $|(R_H - R_K/2)/(R_K/2)| \lesssim 5 \times 10^{-10}$ which is further reduced to about 1×10^{-10} for $B = 10$ T. Note, that previously a comparable performance has only been demonstrated for graphene-based Hall samples at 1.4 K, but not at 4.2 K as in this work [42, 43, 46]. Measurements of the QHR in graphene have reached 1×10^{-9} accuracy of R_H at 7.5 K and 10 K using similar current and field levels which

proves an excellent robustness of the accuracy against temperature increase [43, 47], which was not investigated for our device. Nevertheless, the results demonstrate the high graphene quality and the high potential of the PASG technique with respect to graphene-based electronic devices.

In summary, we have presented a new easy-to-apply graphene fabrication technique in which the sublimation growth is assisted by an extra carbon source from a polymer precursor. The essential step of this mechanism is the stabilization of the SiC surface by enhanced formation of uniformly distributed buffer layer domains from the deposited carbon in the first stage of the thermal process. This is the key to achieve overall suppression of giant step bunching and to enable the use of a larger variety of SiC substrates with different miscut angles. PASG graphene on small miscut substrate shows bilayer-free monolayer coverage, extraordinarily low terrace step heights below 0.75 nm and excellent electronic properties demonstrated by quantum Hall resistance metrology measurements with an unreached accuracy at 4.2 K. Considering the large domain size of undisturbed monolayer graphene and the excellent reproducibility, this method represents the missing part for high yield commercial wafer-scale epitaxial graphene growth and device fabrication.

Methods

Substrate and substrate preparation for PASG

Semi-insulating 6H-SiC(0001) 4″ wafer from II–VI Deutschland with small nominal miscut angles between 0.01° and 0.06° as well as one with a larger miscut of about 0.37° were used. The values for the miscut components provided by the vendor were verified and regularly checked by AFM. The wafer was cut into sample pieces of typically 10 mm × 5 mm. For PASG pure AZ5214E photoresist is used for liquid phase deposition (LPD) of the novolak resin. For LPD the sample was immersed in an ultra-sonic bath of undiluted resist at 30 °C for 10 min in a beaker. To remove the excess polymer from the surface, this step is followed by intensively rinsing the sample with isopropanol for about 1 min using a wash bottle. The application under clean room conditions e.g. yellow light might be important. This results in uniformly distributed droplet-like polymer adsorbate as shown in figure 2(a). Adjusting the time ranges for the deposition and the rinsing step can be used to control the shape and density of the adsorbate. On large miscut substrates a larger amount of polymer adsorbate with increased structure heights (e.g. 20 nm) is favorable compared to small miscut substrates where usually less adsorbate with structure heights similar to figure 2(a) is sufficient. Alternatively, spin coating of a weak solution of 1–4 droplets of AZ-photoresist or PMMA in 50 ml of solvent leads to similar results on most parts of the surface [48, 49]. For spin coating a rotation rate of 6000 rpm and a time of 30 s were used. However, for this method the homogeneity of the polymer adsorbate close to the sample edges appeared to be less compared to LPD.

Buffer layer and graphene growth

For buffer layer and graphene growth the samples were introduced into an inductively heated hot-wall reactor [50]. One or two samples were processed at the same time. The sample is put in a graphite suszeptor adjoined by SiC dummy pieces. Initially, the system is evacuated to 1×10^{-6} mbar at 950 °C for 30 min. The predefinition of the buffer layer was realized by annealing the sample in an argon atmosphere of 1 bar (gas flow of 0 sccm) at temperatures from 1300 to 1500 °C for 5 min. For the subsequent graphene growth the sample was heated (400 K min^{-1}) to a growth temperature of 1750 °C and kept for 5 min before cooling down.

The reproducibility of the PASG method is proven by inspection of more than 50 samples by optical microscopy in high contrast reflection imaging mode [17], 30 by AFM and 5 by Raman mapping where we have obtained comparable results as presented in this publication.

AFM

The Nanostation II AFM from Surface Imaging Systems-SIS (now Bruker) was operated in amplitude-controlled non-contact/intermittent-contact mode. It uses a unique fiber-interferometric detection system that allows absolute measurement of the cantilever oscillation amplitude. The clear material contrasts in the recorded phase images allow distinguishing SiC, buffer layer and graphene surfaces. The AFM probe type is a *PPP-NCLR* PointProbePlus Silicon sensor from Nanosensors.

Raman

Raman measurements were performed using a *LabRAM ARAMIS* spectrometer with an excitation wavelength of 532 nm and an incident excitation power of 10 mW. A piezo stage enables lateral movement with a step-size of 0.2 μm and a lateral resolution of less than 1 μm. Each single spectrum in figure 2(k) is a difference spectrum based on 121 single measurements distributed over an area of 10 μm × 10 μm to reduce noise of which a similarly recorded spectrum of a clean 6H-SiC reference sample is subtracted to remove disturbing overtones of the substrate. The Micro-Raman mappings in figure 3(c) show the distribution of the FWHM value of the characteristic 2*D* peak of graphene [32] which was evaluated by an automated Lorentzian fitting algorithm for each data point.

XPS

The samples were initially heated to 300 °C to remove absorbed contaminations from the sample surface before the measurements were performed in the same UHV environment. The XPS C1s core-level spectra were measured at photon energy of 1486.74 eV which corresponds to the *K*-alpha line of aluminum. The diameter of the sample spot was about 5 mm × 0.5 mm. Charging effects caused by the semi-insulating substrates led to a slight shift of the spectra up to a few eV. The uniform peak-shapes indicate a nondispersive shift which allows an alignment of the spectra by shifting the SiC bulk peak to the well-known position at 283.7 eV [22].

SPA-LEED

The high-resolution LEED experiments were performed with a SPA-LEED system. The diameter of the sample spot was about 1 mm. The LEED images were acquired at 140 eV and 180 eV, which corresponds to a scattering phase of $S = 4.8$ and $S = 5.4$ for the specular spot, respectively.

Electrical measurements

Van der Pauw measurements were performed in a He-flow cryostat and a variable magnetic field up to 0.5 T with an automated measurement system. In order to prevent leakage current through graphene on the edges and backside of the sample a square (almost 5 mm × 5 mm) of monolayer graphene on the SiC (0001) face was isolated using a diamond scriber. The graphene was contacted by softly pressing Au contact pins onto the corners of the sample. The ohmic behavior and the linearity of the Hall curves were checked. The samples were measured directly after growth.

The Hall bar (100 μm × 400 μm) for QHE measurements was fabricated using standard e-beam lithography for the Au/Ti contacts and graphene structuring. For the reduction of the electron concentration by chemical gating the graphene sample was spin coated by a PMMA/MMA copolymer of 55 nm followed by a ZEP520A layer of 300 nm. By UV illumination the electron density was adjusted before the sample was cooled down for measurement. The sample was measured at 4.2 K in a helium cryostat equipped with a superconducting magnet.

Measurements of the longitudinal resistivity ρ_{xx} with the results presented in figure 4(c) followed the established guidelines for the application of the QHE in dc resistance metrology [45]. According to Kirchhoff's law, the longitudinal voltage between two potential contacts on one side of the Hall bar is determined as the difference of two Hall voltages. This is done by measuring the voltage difference between each of them while fixing one potential contact on the other side. For the measurements with the results shown in figure 4(c), the voltage between the contacts 3 and 7 is obtained from Hall measurements choosing two sets of two contact pairs, namely 2 & 3 and 2 & 7 and also 6 & 3 and 6 & 7. The determination of the very small differences between the Hall voltages was possible by including the Hall sample into a cryogenic current comparator-based measurement bridge. Comparisons were performed with a calibrated normal resistor with a nominal value of 100 Ω and a measurement current of 38.74 μA. The resolution of this setup is of the order of 10^{-9} [51].

The precision measurements with the results presented in figure 4(c) followed the established guidelines for the application of the QHE in dc resistance metrology [45]. Additionally, the quantized Hall resistances of the PASG graphene sample was indirectly compared with that of a GaAs-based sample by means of a normal resistor with a nominal value equal to ½ $R_{K\text{-}90}$. The difference between both calibration values for the wire-wound resistor was 6×10^{-10}, the expanded relative uncertainty (also including contributions from the corrections to be applied for the normal resistor's air pressure dependence and its drift over six days) was 9×10^{-10}.

Acknowledgments

We gratefully acknowledge funding by the *School for Contacts in Nanosystems* (*NTH nano*) and the support by the *Braunschweig International Graduate School of Metrology B-IGSM* and *NanoMet*.

Competing financial interests

The authors declare no competing financial interests.

References

[1] Berger C *et al* 2004 Ultrathin epitaxial graphite: 2D electron gas properties and a route toward graphene-based nanoelectronics *J. Phys. Chem.* B **108** 19912–6
[2] Avouris P and Dimitrakopoulos C 2012 Graphene: synthesis and applications *Mater. Today* **15** 86–97
[3] Virojanadara C, Syväjarvi M, Yakimova R, Johansson L, Zakharov A and Balasubramanian T 2008 Homogeneous large-area graphene layer growth on 6H-SiC(0001) *Phys. Rev.* B **78** 1–6
[4] Emtsev K V *et al* 2009 Towards wafer-size graphene layers by atmospheric pressure graphitization of silicon carbide *Nat. Mater.* **8** 203–7
[5] de Heer W A, Berger C, Ruan M, Sprinkle M, Li X, Hu Y, Zhang B, Hankinson J and Conrad E 2011 Large area and structured epitaxial graphene produced by confinement controlled sublimation of silicon carbide *Proc. Natl Acad. Sci.* **108** 16900–5
[6] Real M A, Lass E A, Liu F-H, Shen T, Jones G R, Soons J A, Newell D B, Davydov A V and Elmquist R E 2013 Graphene epitaxial growth on SiC(0001) for resistance standards *IEEE Trans. Instrum. Meas.* **62** 1454–60
[7] Virojanadara C, Yakimova R, Osiecki J R, Syväjärvi M, Uhrberg R I G, Johansson L I and Zakharov A A 2009 Substrate orientation: a way towards higher quality monolayer graphene growth on 6H-SiC(0001) *Surf. Sci.* **603** L87–90
[8] Al-Temimy A, Riedl C and Starke U 2009 Low temperature growth of epitaxial graphene on SiC induced by carbon evaporation *Appl. Phys. Lett.* **95** 231907

[9] Moreau E, Ferrer F J, Vignaud D, Godey S and Wallart X 2010 Graphene growth by molecular beam epitaxy using a solid carbon source *Phys. Status Solidi* **207** 300–3

[10] Michon A, Ýzian S, Ouerghi A, Zielinski M, Chassagne T and Portail M 2010 Direct growth of few-layer graphene on 6H-SiC and 3C-SiC/Si via propane chemical vapor deposition *Appl. Phys. Lett.* **97** 171909

[11] Strupinski W *et al* 2011 Graphene epitaxy by chemical vapor deposition on SiC *Nano Lett.* **11** 1786–91

[12] Eriksson J, Pearce R, Iakimov T, Virojanadara C, Gogova D, Andersson M, Syväjärvi M, Lloyd Spetz A and Yakimova R 2012 The influence of substrate morphology on thickness uniformity and unintentional doping of epitaxial graphene on SiC *Appl. Phys. Lett.* **100** 241607

[13] Ji S-H, Hannon J B, Tromp R M, Perebeinos V, Tersoff J and Ross F M 2012 Atomic-scale transport in epitaxial graphene *Nat. Mater.* **11** 114–9

[14] Low T, Perebeinos V, Tersoff J and Avouris P 2012 Deformation and scattering in graphene over substrate steps *Phys. Rev. Lett.* **108** 1–4

[15] Yakes M K, Gunlycke D, Tedesco J L, Campbell P M, Myers-Ward R L, Eddy C R, Gaskill D K, Sheehan P E and Laracuente A R 2010 Conductance anisotropy in epitaxial graphene sheets generated by substrate interactions *Nano Lett.* **10** 1559–62

[16] Schumann T, Friedland K-J, Oliveira M, Tahraoui A, Lopes J and Riechert H 2012 Anisotropic quantum Hall effect in epitaxial graphene on stepped SiC surfaces *Phys. Rev.* B **85** 235402

[17] Yager T *et al* 2013 Express optical analysis of epitaxial graphene on SiC: impact of morphology on quantum transport *Nano Lett.* **13** 4217–23

[18] Chua C *et al* 2014 Quantum Hall effect and quantum point contact in bilayer-patched epitaxial graphene *Nano Lett.* **14** 3369–73

[19] Kruskopf M *et al* 2015 Epitaxial graphene on SiC: modification of structural and electron transport properties by substrate pretreatment *J. Phys.: Condens. Matter* **27** 185303

[20] Ferrari A and Robertson J 2000 Interpretation of Raman spectra of disordered and amorphous carbon *Phys. Rev.* B **61** 14095–107

[21] Ko T-H, Kuo W-S and Chang Y-H 2000 Raman study of the microstructure changes of phenolic resin during pyrolysis *Polym. Compos.* **21** 745–50

[22] Emtsev K V, Speck F, Seyller T and Ley L 2008 Interaction, growth, and ordering of epitaxial graphene on SiC{0001} surfaces: a comparative photoelectron spectroscopy study *Phys. Rev.* B **77** 1–10

[23] Díaz J, Paolicelli G, Ferrer S and Comin F 1996 Separation of the sp3 and sp2 components in the C1s photoemission spectra of amorphous carbon films *Phys. Rev.* B **54** 8064–9

[24] Mildner D F R and Carpenter J M 1982 On the short range atomic structure of non-crystalline carbon *J. Non. Cryst. Solids.* **47** 391–402

[25] Schueller O and Brittain S 1997 Fabrication and characterization of glassy carbon MEMS *Chem. Mater.* **4756** 1399–406

[26] Hiura H, Ebbesen T W, Tanigaki K and Takahashi H 1993 Raman studies of carbon nanotubes *Chem. Phys. Lett.* **202** 509–12

[27] Escribano R, Sloan J J, Siddique N, Sze N and Dudev T 2001 Raman spectroscopy of carbon-containing particles *Vib. Spectrosc.* **26** 179–86

[28] Fromm F, Oliveira M H Jr, Molina-Sánchez A, Hundhausen M, Lopes J M J, Riechert H, Wirtz L and Seyller T 2013 Contribution of the buffer layer to the Raman spectrum of epitaxial graphene on SiC(0001) *New J. Phys.* **15** 043031

[29] Jeong H and Weeks J D 1998 Two-dimensional dynamical model for step bunching and pattern formation induced by surface reconstruction *Phys. Rev.* B **57** 3939–48

[30] Riedl C, Coletti C and Starke U 2010 Structural and electronic properties of epitaxial graphene on SiC(0 0 0 1): a review of growth, characterization, transfer doping and hydrogen intercalation *J. Phys. D: Appl. Phys.* **43** 374009

[31] Hannon J B and Tromp R M 2008 Pit formation during graphene synthesis on SiC(0001): in situ electron microscopy *Phys. Rev.* B **77** 241404

[32] Lee D S, Riedl C, Krauss B, von Klitzing K, Starke U and Smet J H Raman spectra of epitaxial graphene on SiC and of epitaxial graphene transferred to SiO_2 *Nano Lett.* **8** 4320–5

[33] Hannon J B, Copel M and Tromp R M 2011 Direct measurement of the growth mode of graphene on SiC(0001) and SiC(0001[over ¯]) *Phys. Rev. Lett.* **107** 166101

[34] Fromm F J 2015 Raman-spektroskopie an epitaktischem graphen auf siliziumkarbid (0001) *PhD Thesis* Technische Universität Chemnitz (http://nbn-resolving.de/urn:nbn:de:bsz:ch1-qucosa-165167)

[35] Oliveira M H, Schumann T, Ramsteiner M, Lopes J M J and Riechert H 2011 Influence of the silicon carbide surface morphology on the epitaxial graphene formation *Appl. Phys. Lett.* **99** 111901

[36] Röhrl J, Hundhausen M, Emtsev K V, Seyller T, Graupner R and Ley L 2008 Raman spectra of epitaxial graphene on SiC(0001) *Appl. Phys. Lett.* **92** 201918

[37] Ohta T, Bartelt N C, Nie S, Thürmer K and Kellogg G L 2010 Role of carbon surface diffusion on the growth of epitaxial graphene on SiC *Phys. Rev.* B **81** 121411

[38] Tedesco J L, Vanmil B L, Myers-Ward R L, McCrate J M, Kitt S A, Campbell P M, Jernigan G G, Culbertson J C, Eddy C R and Gaskill D K 2009 Hall effect mobility of epitaxial graphene grown on silicon carbide *Appl. Phys. Lett.* **95** 122102

[39] Pan W, Howell S W, Ross A J, Ohta T and Friedmann T A 2010 Observation of the integer quantum Hall effect in high quality, uniform wafer-scale epitaxial graphene films *Appl. Phys. Lett.* **97** 252101

[40] Jabakhanji B *et al* 2014 Tuning the transport properties of graphene films grown by CVD on SiC(0001): effect of in situ hydrogenation and annealing *Phys. Rev.* B **89** 085422

[41] Lara-Avila S, Moth-Poulsen K, Yakimova R, Bjørnholm T, Fal'ko V, Tzalenchuk A and Kubatkin S 2011 Non-volatile photochemical gating of an epitaxial graphene/polymer heterostructure *Adv. Mater.* **23** 878–82

[42] Lafont F *et al* 2015 Quantum Hall resistance standards from graphene grown by chemical vapour deposition on silicon carbide *Nat. Commun.* **6** 6806

[43] Ribeiro-Palau R *et al* 2015 Quantum Hall resistance standard in graphene devices under relaxed experimental conditions *Nat. Nanotechnol.* **10** 965–71

[44] Van Der Wel W, Harmans C J P M and Mooij J E 1988 A geometric explanation of the temperature dependence of the quantised Hall resistance *J. Phys. C: Solid State Phys.* **21** L171–5

[45] Delahaye F and Jeckelmann B 2003 Revised technical guidelines for reliable dc measurements of the quantized Hall resistance *Metrologia* **40** 217–23

[46] Tzalenchuk A, Lara-Avila S, Kalaboukhov A, Paolillo S, Syväjärvi M, Yakimova R, Kazakova O, Janssen T J B M, Fal'ko V and Kubatkin S 2010 Towards a quantum resistance standard based on epitaxial graphene *Nat. Nanotechnol.* **5** 186–9

[47] Janssen T J B M, Williams J M, Fletcher N E, Goebel R, Tzalenchuk A, Yakimova R, Lara-Avila S, Kubatkin S and Fal'ko V I 2012 Precision comparison of the quantum Hall effect in graphene and gallium arsenide *Metrologia* **49** 294–306

[48] Kruskopf M and Pierz K 2015 Verfahren zum Herstellen von Graphen *Europen Patent* EP15172720.3-1355

[49] Pakdehi D M 2015 Epitaxial graphene on 4H- and 6H-SiC: growth optimization and characterization *Msc Thesis* Bremen City University of Applied Sciences

[50] Ostler M, Speck F, Gick M and Seyller T 2010 Automated preparation of high-quality epitaxial graphene on 6H-SiC (0001) *Phys. Status Solidi* **247** 2924–6

[51] Goebel R, Fletcher N, Rolland B, Bundesanstalt P and Em-k O B 2014 Comparison of quantum Hall effect resistance standards of the PTB and the BIPM on-going comparison report on the 2013 on-site comparison final report July 2014 comparison of quantum Hall effect resistance standard *Metrologia* **51** 01011